

## THE COALESCENCE OF BUBBLES - A NUMERICAL STUDY

**Li Chen, Yuguo Li and Richard Manasseh**  
*Advanced Fluid Dynamics Laboratory  
CSIRO Building, Construction and Engineering  
Highett, Victoria 3190, Australia*

### Abstract

The dynamics of bubble coalescence is studied using a robust numerical model for a multiphase flow system with interfaces. The effects of liquid viscosity and surface tension on bubble coalescence, for which Reynolds number ranges from 10 to 100 and Bond number ranges from 5 to 50, are investigated. It is shown that the numerical model used in this study can accurately capture the complex topological changes during the coalescence. The predicted behaviour of bubble coalescence is in reasonable agreement with our experimental observation. It is found that with a high Reynolds number (low viscosity) a strong liquid jet formed behind the leading bubble inhibits the approach of the following bubble. Hence coalescence does not occur or is postponed. A lower surface tension results in an earlier coalescence because of severe stretching of the interface.

### 1. Introduction

The dynamics of bubble coalescence plays an important role in many engineering processes. For example, in mixing, bubbles or drops can generate large changes in interfacial areas through the action of vorticity via stretching, tearing and folding which facilitates the mixing processes. A good understanding of the fundamental mechanism of multiple bubble coalescence can be crucial in maintaining the dispersion process. The dynamics of liquid drop coalescence has been addressed by many researchers, such as Muccucci (1969), Chi and Leal (1989) and Basaran (1992). Limited theoretical and experimental studies of gas bubble coalescence were done by Narayanan et al (1974), Bhaga and Weber (1980), Oolman and Blanch (1986), Egan and Tobias (1994) and Stover et al (1997). Most of their studies focused on the experimental investigation. Stover et al (1997) adopted a finite-element method to study small bubble coalescence and the simulated results were used to validate their experimental observation. In their study, they focused on the interfacial dynamics after two bubbles touched.

Discontinuous fluid properties in a flow system can produce a complex flow structure with rich physical length scales, which presents both computational and experimental challenges. Numerically, a robust algorithm for solving multi-phase flows with an accurate representation of interfaces is required to accommodate the complex topological changes in bubble coalescence.

In this paper, gas bubble coalescence has been studied using our modified VOF method (Chen et al. 1996) associated with a semi-implicit algorithm for Navier-Stokes equations. The effects of liquid viscosity and surface tension force on the coalescence are also investigated

### 2. Problem Formulation

Consider two spherical gas bubbles, rising through a viscous liquid (see Figure 1) in a closed cylinder. The two bubbles are initially stationary and the coalescence of the two bubbles may occur while they are rising due to the buoyancy force.

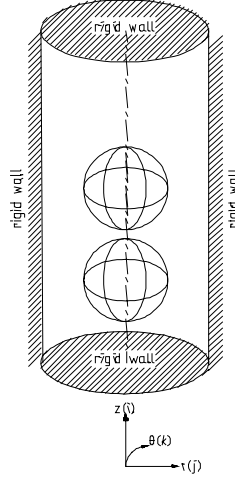


**Figure 1:** Schematic description of the problem

The motion of the two bubbles can be described by the Navier-Stokes equation, which is written in a non-dimensional form as

$$\nabla \cdot \mathbf{U} = 0 \quad (1)$$

$$\begin{aligned} \frac{\partial(\rho\mathbf{U})}{\partial t} + \nabla \cdot (\rho\mathbf{U} \otimes \mathbf{U}) = -\nabla p + \rho\mathbf{g} + \\ \frac{1}{\text{Re}} \nabla \cdot [\mu(\nabla\mathbf{U} + \nabla\mathbf{U}^T)] + \frac{1}{\text{Bo}} \mathbf{F}_{sv}, \end{aligned} \quad (2)$$

with scales

$$\begin{aligned} p^* = \frac{p}{p_{ref}}, \mathbf{U}^* = \frac{\mathbf{U}}{u_{ref}}, \mathbf{x}^* = \frac{\mathbf{x}}{R_0}, \mathcal{t} = \frac{t}{t_{ref}}, \\ \rho^* = \frac{\rho}{\rho_{ref}}, \mu^* = \frac{\mu}{\mu_{ref}}, \sigma^* = \frac{\sigma}{\sigma_{ref}}, \end{aligned} \quad (3)$$

in which

$$u_{ref} = \sqrt{gR_0}, p_{ref} = \rho_{ref} u_{ref}^2. \quad (4)$$

Note that \* is omitted in equations (1) and (2) for convenience.  $\otimes$  denotes the inner product of tensors,  $\mathbf{U}(u_r, u_\theta, u_z)$  is the fluid velocity in  $\mathbf{x}(r, \theta, z)$ ,  $\rho$  the density,  $\mu$  the dynamic viscosity,  $p$  the pressure,  $\mathbf{g}(0, 0, g)$  the gravity vector,  $R_0$  initial bubble radius, and  $\mathbf{F}_{sv}$  the volume form of the surface tension force. The subscript, *ref*, stand for a reference value, and here, liquid properties are adopted as reference properties. Reynolds and Bond numbers are defined by

$$\text{Re} = \frac{\rho_f g^{1/2} R_0^{3/2}}{\mu_{ref}}, \text{Bo} = \frac{\rho_f g R_0^2}{\sigma},$$

and

$$\rho(\mathbf{x}, t) = F(\mathbf{x}, t)\rho_f + [1 - F(\mathbf{x}, t)]\rho_g, \quad (5)$$

$$\mu(\mathbf{x}, t) = F(\mathbf{x}, t)\mu_f + [1 - F(\mathbf{x}, t)]\mu_g, \quad (6)$$

where  $F$  is the local volume fraction of one fluid. Its value may be unity in the liquid phase and zero in the gas phase if a gas-liquid two-phase system is involved. A value between 1 and 0 indicates a density interface. The last term of equation (2) is the surface tension force, which exists only at the interface and is modelled by the continuum surface tension force (CSF) method developed by Brackbill et al (1992). In this model, an interface is interpolated as a transient region with a finite thickness. Thus the surface tension force localised in this region can be converted into a volume force with the help of a Dirac delta function concentrated on the surface. The surface tension force is written as

$$\mathbf{F}_{sv} = \sigma\kappa(\mathbf{x}) \frac{\nabla\tilde{c}(\mathbf{x})}{[\tilde{c}]}, \quad (7)$$

in which

$$\kappa = -(\nabla \cdot \hat{\mathbf{n}}), \quad (8)$$

from the definition of a unit normal vector to a surface

$$\hat{\mathbf{n}} = \frac{\nabla \tilde{c}}{|\nabla \tilde{c}|}, \quad (9)$$

where  $\tilde{c}$  in the above equations is a colour function and  $[\tilde{c}]$  is the difference of the colour function between two phases.

It is noted that Equations (5) and (6) represent discontinuous properties of fluid, which imply an interface between two-phase fluids, and they can be used to monitor the dynamics of the interface. However, when a large discontinuity is involved, for example a discontinuity of 850 in density ratio exists for a water-air system, numerical difficulties may arise in identifying an ‘exact’ interface. Thus, instead of solving the density transport equation directly, the volume fraction of liquid,  $F$ , is used to identify an interface. The transport of the  $F$  function is governed by

$$\frac{\partial F}{\partial t} + \nabla \cdot (\mathbf{U}F) = 0 \quad (11)$$

Also, the colour function,  $\tilde{c}$ , in Equations (7) and (9) can be replaced by  $F$ . Now suitable initial and boundary conditions are required. In the case studied in this paper, an initially spherical gas bubble is located on the axis of a vertical cylinder filled with a stationary liquid. The boundary conditions are  $\mathbf{U} = 0$  at the walls. The bubble is initially at rest.

### 3. Numerical Method

A control volume technique is used to discretise the PDEs. The computational domain is divided into a number of non-overlapping control-volumes and all variables are defined at the centre of the control volume. Such a collocated arrangement of the grid may reduce the discretization accuracy of the diffusive term, but it has advantages, such as an accurate representation of flux and source terms.

The diffusion terms are discretized by a second-order central differencing scheme. The convection terms are discretised with a third-order upwind-biased scheme and implemented with the deferred-correction method. Generally, when a single bubble rises due to the buoyancy force, a tongue of liquid jet is induced that pushes into the bubble from below. Deformations of the bubble occur. For multiple bubbles, similar behaviour is expected. The use of a higher-order convection scheme is necessary to catch the liquid jet accurately with a moderate number of grid points. Comparing the conventional first-order hybrid scheme with the third-order scheme, it has been found that the upwind-biased scheme gives a better resolution of the liquid jet behind two bubbles. The flux at the faces of a control volume is calculated by the Rhie-Chow’s interpolation. This technique effectively overcomes the difficulty of the decoupling between pressure and velocity raised by a linear interpolation and guarantees a global mass conservation. The surface tension force is linearised by a 27-point stencil for a three-dimensional surface. The detail of numerical implementations can be found in Chen et al (1996, 1997).

To capture the sophisticated dynamics of an interface, an accurate technique is needed to solve equation (11). There are many different algorithms to solve this equation, for example, the Lagrangian finite-element method of Unverdi and Tryggvason (1992) and the MAC-type technique of Rider et al (1995). However, the VOF method pioneered by Hirt and Nichols (1982) is still widely used due to the simplicity in its implementation. In this study, a modified line constant VOF method is used (see Chen et al. 1996).

A semi-implicit scheme is used to solve equation (2) for the velocity field and the SIMPLE method is adopted for the velocity-pressure coupling. The resultant non-symmetrical system of linear equations arising from the momentum equation is solved by SIP. The symmetric system due to pressure correction is solved by the Conjugate Gradient method with the Incomplete Cholesky preconditioning.

### 4. Results and Discussion

A grid-independent test was carried out on the axisymmetric rise of a single bubble in a liquid with three different meshes ( $N_z$  by  $N_r$ ): 54 by 17, 108 by 34 and 216 by 68, which correspond to 145, 578 and 2312 grid points in the rectangle containing the hemisphere region. It was found that the 108 by 34 mesh produces a nearly grid-independent solution. This grid size will be used in all other runs.

#### 4.1 The Behaviour of Bubble Coalescence

Generally, when a single bubble rises due to the buoyancy force, the pressure at the lower surface of the bubble is higher than that at the top surface of the bubble. A vortex sheet developed at the surface of the bubble has a sense of rotation, which induces a tongue of liquid that pushes into the bubble from below. Deformations of the bubble occur. For multiple bubbles, similar behaviour is expected but the deformation and fragmentation of surfaces are much more complex.

The behaviour of bubble coalescence in a viscous liquid is shown in Figure 2 with parameters:  $Re=12$ ,  $Bo=5$  and  $\rho_f/\rho_g=1000$  and  $\mu_f/\mu_g=100$ , which gives an equivalent Morton number ( $M = Bo^3/Re^4$ ) of  $M=4.1 \times 10^{-3}$ . This is just above the critical Morton number for bubble coalescence (Bhaga and Weber 1980). This figure plots the velocity field and three contour lines of function  $F$ , 0.1, 0.5 and 0.9. When they start to rise, two bubbles become ellipsoids due to a pressure difference between the top and bottom surfaces of the bubbles. The liquid jet formed behind the leading bubble induces a severe deformation of the following bubble, giving it a pear-like shape (Figures 2a, b). Once two bubbles are approaching (Figure 2b), the following bubble accelerates. As time progresses, the two bubbles start to touch, as may be seen in Figure 2c, leaving a mushroom-like structure. The surface tension force is decreased, and then a further fragmentation occurs. A larger spherical cap is obtained, as may be seen in Figure 2d. A detailed study of the motion of such a single bubble in a viscous liquid, such as the formation of a toroidal bubble, can be found in Chen et al (1998).

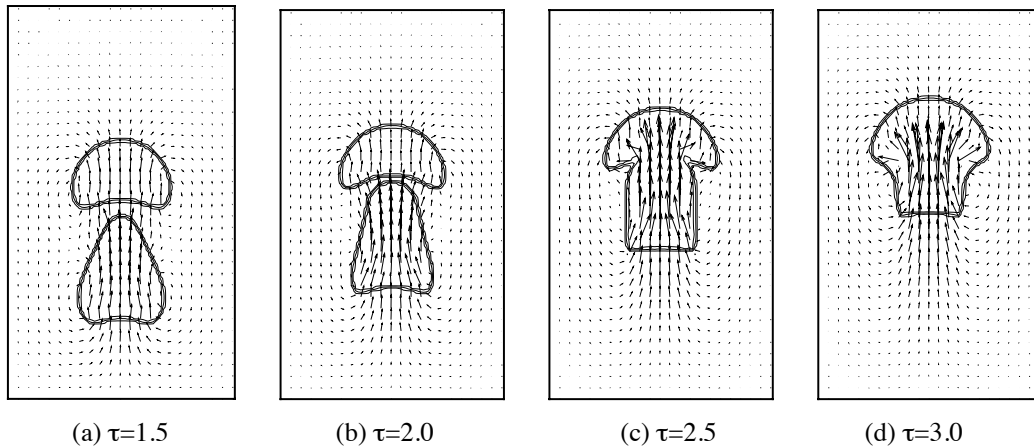


**Figure 2:** Predicted axisymmetric coalescence of two gas bubbles in a viscous liquid ( $Re=12$ ,  $Bo=5$ ,  $M=4.1 \times 10^{-3}$ ,  $\rho_f/\rho_g=1000$ ,  $\mu_f/\mu_g=100$ ,  $z/R_0=0.36$ )

It can be seen that the liquid circulation around the bubble produces a jet to push in the lower surface of both leading and following bubbles and the deformations of the bubbles occur (Figure 2a). Due to the impact of the following bubble, the vortex around the leading bubble is terminated and instead, a big circulation around two bubbles as a whole is gradually formed (Figures 2b, c and d). Therefore the liquid jet behind the leading bubble may be slightly smeared and a spherical-cap-shaped leading bubble is observed (Figure 2b). The liquid jet, in another words the pressure, behind the leading bubble controls the entrainment of the following bubble by promoting a slight acceleration and elongation of the following bubble, which eventually causes the coalescence. After the two bubbles touch, because the surface tension always acts as a force reducing surface energy, the lower surface of the merged bubble is accelerated and a larger spherical cap is obtained (Figures 2c,d). It seems that the following bubble has very little effect on the travel of the leading bubble, which can be seen in Figure 3 by the nearly straight line of the leading bubble position history before the coalescence occurs. (In this figure, the sudden drop of the leading bubble's position or the end of the following bubble's line indicates a coalescence.) This agrees with Bhaga and Weber (1980). A small acceleration of the following bubble can be seen by its position plot having a slight upturn at  $\tau=0.9$ . The merged bubble travels faster than the small one, as may be seen by a bigger slope of the solid line after  $\tau=2.0$  in Figure 3. It can also be seen that the contour lines of  $F$  in Figure 2 show an accurate representation of the bubbles with minimum numerical diffusion.

An experiment was carried out with a glycerin liquid with  $\rho_f \approx 1220 \text{ kgm}^{-3}$ ,  $\mu_f = 0.11 \text{ kgm}^{-1}\text{s}^{-1}$  and  $\sigma = 0.066 \text{ Nm}^{-1}$  to validate the numerical simulation, as may be seen in Figure 4. The experimental method is given in Manasseh et al (1998). The equivalent radius of a spherical bubble was determined from the acoustic frequency of bubble oscillation (Manasseh, 1997). These properties give equivalent non-dimensional parameters:  $Bo=5$ ,  $M=4.1 \times 10^{-3}$  and  $\rho_f/\rho_g \approx 1000$  with a 10% error in both density and viscosity estimation. The similarity of the bubble coalescence between the predicted and experimental results can be seen from Figures 2 and 4. The experimental result for the average rise velocity, with reference to the leading bubble centre before coalescence, gives  $0.3 \text{ ms}^{-1}$ , while the numerical simulation gives  $0.24 \text{ ms}^{-1}$ . This gives an error of 20%. The differences between the numerical and experimental following bubbles appear mostly in the first two frames. This is due to the different initial conditions. Given the somewhat different initialisation and uncertain fluid properties in experiment, the agreement between the results may be considered reasonable.

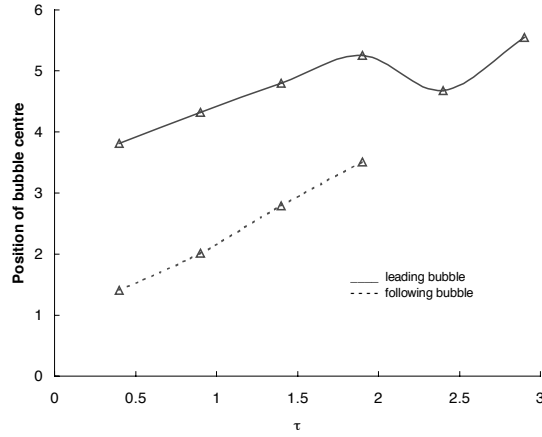


**Figure 3:** The position of the two bubble centres as a function of time ( $Re=12$ ,  $Bo=5$ ,  $M=4.1 \times 10^{-3}$ ,  $\rho_f/\rho_g=1000$ ,  $\mu_f/\mu_g=100$ ,  $z/R_0=0.36$ )

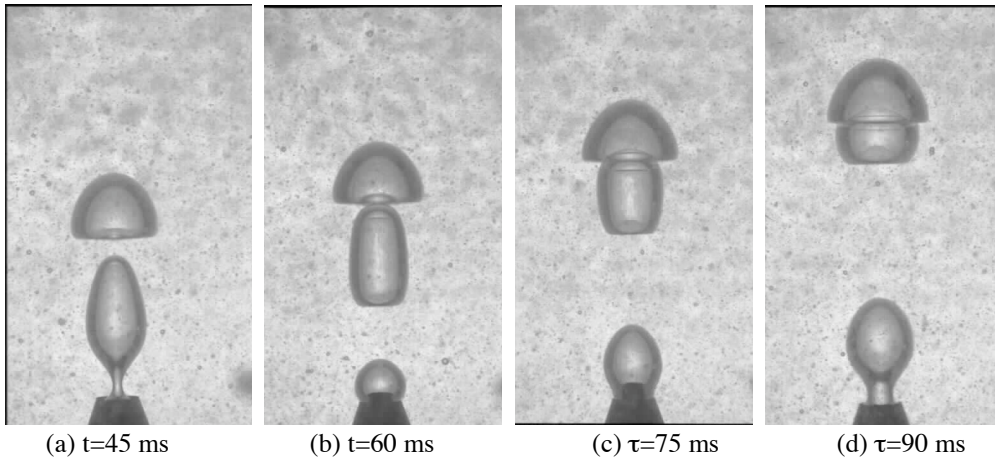


**Figure 4:** Experimental observation of the axisymmetric coalescence of two gas bubbles in a glycerin liquid ( $M=4.1 \times 10^{-3}$ ,  $Bo=5$ ,  $\rho_f/\rho_g \approx 1000$ )

#### 4.2 The Role of Surrounding Liquid Viscosity on Bubble Coalescence

The effect of liquid viscosity on bubble coalescence is illustrated in Figure 5, by varying Reynolds number from 100 to 10 whilst keeping the remaining parameters unchanged as  $Bo=5$ ,  $\rho_f/\rho_g=100$  and  $\mu_f/\mu_g=100$ . These correspond to Morton numbers of  $M=1.25 \times 10^{-6}$  and  $M=1.25 \times 10^{-2}$  respectively. Here a low density ratio is used for computational efficiency without losing the physics. Again, velocity fields and three contour lines of function  $F$ , 0.1, 0.5 and 0.9, are plotted for two different Reynolds numbers at various times. For a higher Reynolds number (small viscosity in Figure 5a), a stronger jet behind the bubbles results which may be seen by comparing Figures 5a and 5b. A more severe deformation of both leading and following bubbles is obtained. It is the jet behind a bubble that is responsible for the deformation of a single bubble in a liquid (Chen et al 1998). At a higher  $Re$  number, there are a stronger vortex around the leading bubble and a stronger jet, as may be seen from Figures 5a at  $\tau=1.0$ ,  $\tau=1.5$  and  $\tau=2.0$ . This causes a higher pressure in the wake of the leading bubble. Hence the following bubble is prevented from approaching the leading bubble, precluding coalescence, as may be seen from the vector plot in Figure 5a. This gives a weak interaction between the two bubbles, and thus no significant acceleration of the following bubble is obtained. With a high surface tension ( $Bo=5$ ), the two bubbles travelled separately. This is shown in Figure 6 by the pair of nearly parallel lines with  $Re=100$  after  $\tau=1.5$  for the bubble-centre position histories.

The effect of the leading bubble on the shape development of the following bubble is obvious (Figure 5a at  $\tau=1.5$  and  $\tau=2.0$ ). The top of the following bubble expands while it approaches the leading bubble and a hat-type bubble is obtained (Figure 5a,  $\tau=2.5$ ). This is due to the vortex ring in the wake of the leading bubble. On the other hand, the weak vortex around the leading bubble at a low  $Re$  number is easily broken (Figure 5b,  $\tau=2.0$  and  $\tau=2.5$ ) and the impact of the liquid induced by the following bubble on the jet behind the leading bubble is relatively significant. As a result, the leading bubble rises slowly, and the top of the following bubble stretches slowly, leading to coalescence, as may be seen in Figure 6 for  $Re=10$ .

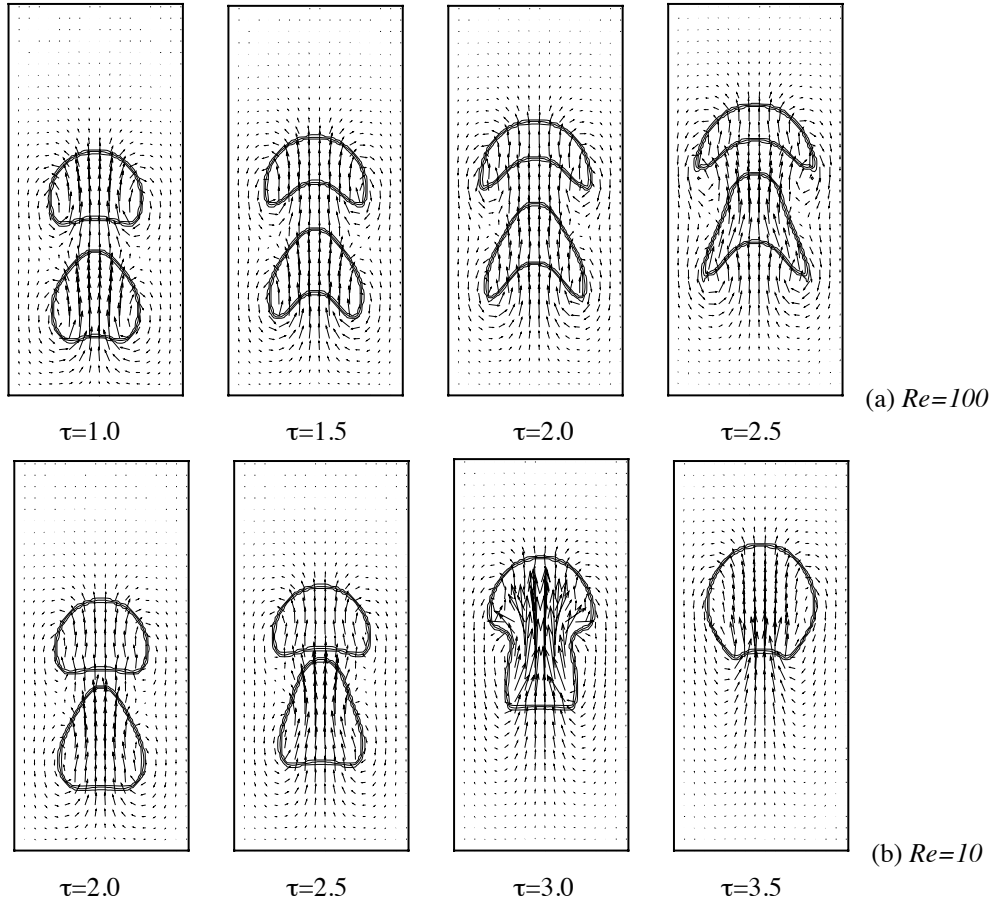


**Figure 5:** Velocity field and three contours of  $F$  of the values of 0.1, 0.5 and 0.9 with different Reynolds numbers (a)  $Re=100$  and (b)  $Re=10$  ( $Bo=5$ ,  $\rho_f/\rho_g=100$ ,  $\mu_f/\mu_g=100$ )

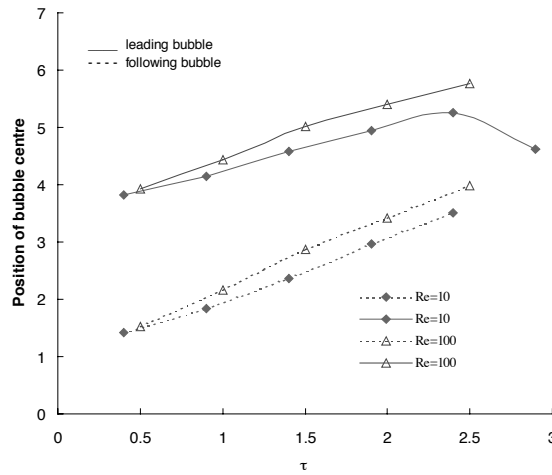


**Figure 6** Effect of Reynolds number on the bubble position history ( $Bo=5$ ,  $\rho_f/\rho_g=100$ ,  $\mu_f/\mu_g=100$ )

### 4.3 The Role of Surface Tension Force on Bubble Coalescence

The effect of Bond number on bubble coalescence is shown in Figure 7 by a three-dimensional plot. The vertical velocity profile along the  $z$ -axis is shown in Figure 8. At a high Bond number (low surface tension), the two bubbles deformed more while approaching and a slightly stronger liquid jet at the beginning of their rise can be seen in Figure 8. In this figure, a value of unity of  $F$  represents the liquid; a value of zero represents the gas and in-between represents an interface. The bubbles with a low surface tension ( $Bo=50$ , open circles) merge as early as  $\tau=2.0$  but with a high surface tension ( $Bo=5$ , solid circles) coalescence is postponed to  $\tau=3.0$ .

A high surface tension results in a weak liquid jet behind both bubbles and a slightly slow rise of the two bubbles. This is shown in Figure 9 by the bubble centre position as a function of time. In addition, the surface

tension force is always trying to maintain a shape having a minimum surface energy, which makes the stretching of the top surface of the following bubble harder. These effects all lead to a late coalescence.

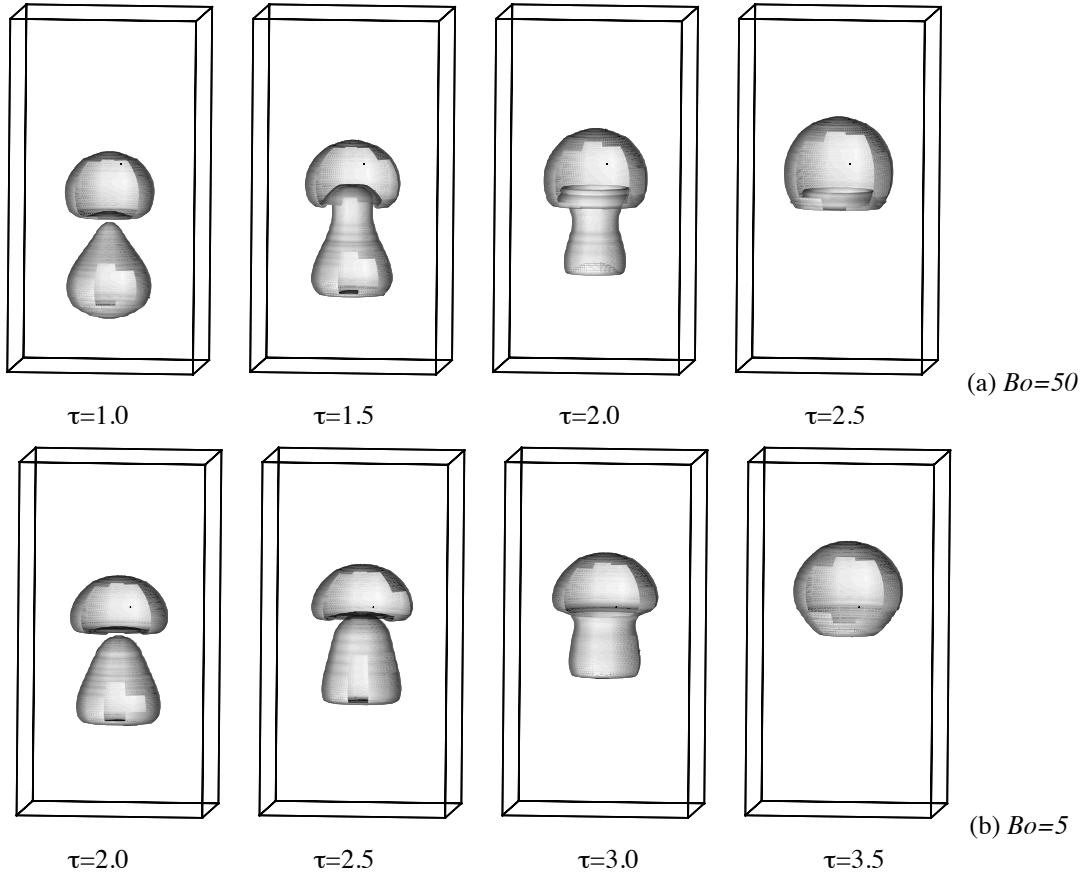


**Figure 7:** Development of bubble coalescence with different Bond numbers: (a)  $Bo=50$  and (b)  $Bo=5$  ( $Re=10$ ,  $\rho_f/\rho_g=850$ ,  $\mu_f/\mu_g=100$ )

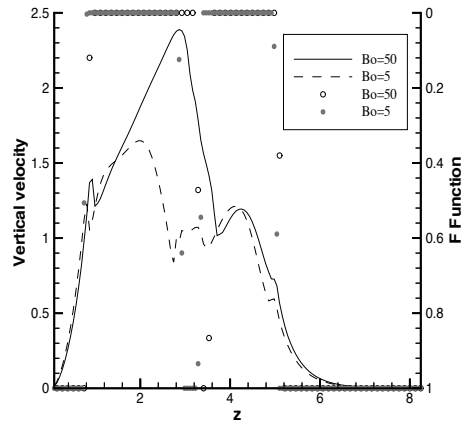


**Figure 8:** Vertical velocity profile along the  $z$ -axis (line) and volume fraction  $F$  (circle) for different Bond numbers ( $Re=10$ ,  $\rho_f/\rho_g=850$ ,  $\mu_f/\mu_g=100$ ,  $\tau=1.0$ )

## 5. Conclusion

The dynamics of bubble coalescence has been studied using a robust numerical model for a two-phase fluid system with interfaces. An experimental validation has been carried out, and the predicted behaviour of bubble coalescence is in reasonable agreement with our experimental observation.

The effects of liquid viscosity and surface tension on the coalescence have been investigated. It has been found that the interaction between the leading and following bubbles depends mainly on the liquid viscosity. The higher the liquid viscosity, the easier the bubbles interact. Therefore, bubble coalescence is more likely for high viscosity. On the other hand, for low viscosity, the liquid jet behind the leading bubble becomes stronger which

prevent the bubble interaction. A postponed or non-coalescence is obtained. Regarding the surface tension effect, high surface tension results in a weak liquid jet, and the resultant high surface tension force prohibits the surface stretching. Therefore, a late coalescence is obtained.

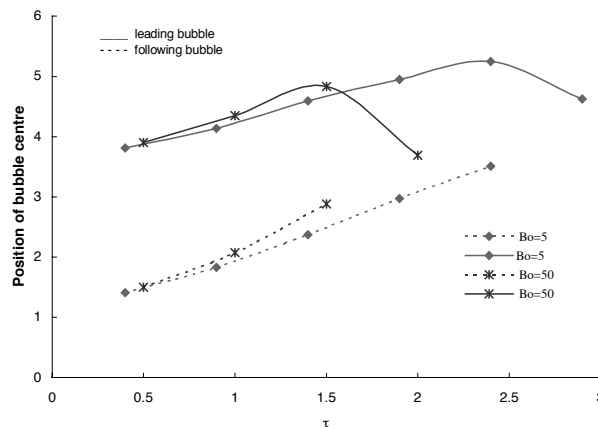


**Figure 9** Effect of surface tension force on the centre positions of leading and following bubbles ( $Re=10$ ,  $\rho_f/\rho_g=850$ ,  $\mu_f/\mu_g=100$ )

## 6. Acknowledgments

The original code used in this study was developed by the first author in UNSW, Sydney, under the supervision of Professors J. A. Reizes and E. Leonardi.

## 7. References

- Basaran, O.A., 'Nonlinear oscillations of viscous liquid drops,' *J. Fluid Mech.*, 241, 169-198, 1992.
- Bhaga, D. and Weber, M.E., 'In-line interaction of a pair of bubbles in a viscous liquid', *Chem. Eng. Sci.*, 35, 2467-2474, 1980.
- Brackbill, J.U., Kothe, D.B., and Zemach, C., 'A continuum method for modeling surface tension,' *J. Comp. Phys.*, 100, 335-354, 1992.
- Chen, L., Garimella, S.V., Reizes, J. A., and Leonardi, E., 'Analysis of bubble rise using the VOF Method: I isolated bubbles', *ASME Proceedings of the 31st NHT Conference*, Houston, 4, 161-173, 1996.
- Chen, L. and Li, Y., 'A numerical simulation of a two phase flow', *MODSIM 97, Proceedings of International Congress on Modelling and Simulation*, Hobart, Australia, 1, 165-170, December 8-11, 1997.
- Chen, L., Garimella, S.V., Reizes, J.A. and Leonardi, E. 'The development of a bubble rising in a viscous liquid', to appear in *J. Fluid Mech.*, 1998.
- Chi, B.K. and Leal, L.G., 'A theoretical study of the motion of a viscous drop towards a fluid interface at low Reynolds number', *J. Fluid Mech.* 201, 123-146, 1989.
- Egan, E.W. and Tobias, C.W., 'Measurement of interfacial re-equilibration during hydrogen bubble coalescence', *J. Electrochem. Soc.*, 141, 1118-1126, 1994.
- Hirt, C. W. and Nichols, B.D., 'Volume of Fluid (VOF) Method for the Dynamics of Free Boundaries', *J. Comp. Phys.*, 39, 201-225, 1982.
- Maccucci, G., 'A Theory of Coalescence', *Chem. Eng. Sci.*, 24, 975-???, 1969.
- Manasseh, R., 'Acoustic Sizing of Bubbles at Moderate to High Bubbling Rates', *Exptl. Fluid. & Thermal Sic. J. Edition for 4<sup>th</sup> Word Conference on Experimental. Heat Transfer, Fluid Mechanics and Thermodynamics*, Brussels, June 2-6, 1997.
- Manasseh, R., Yoshida, S. and Rudman, M., 'Bubble formation processes and bubble acoustic signals", *ICMF'98*, France, June 8-12, 1998.
- Narayanan, S., Goossens, H.J. and Kossen, N.W.F., 'Coalescence of two bubbles rising in line at low Reynolds numbers', *Chem. Eng. Sci.*, 29, 2071-2082, 1974.
- Oolman, T.O. and Blanch, H.W., 'Bubble coalescence in stagnant Liquids', *Chem. Eng. Commun.*, 43, 237-261, 1986.
- Rider, W.J., Kothe, D.B., Mosso, J. and Cerutti, J.H., 'Accurate solution algorithms for incompressible multiphase flows', *AIAA-95-0699*, 1-17, 1995.
- Stover, L.R., Tobias, C.W. and Denn, M.M., 'Bubble coalescence dynamics', *AIChE Journal*, 43, 2385-2392, 1997.
- Unverdi, S.O. and Tryggvason, G.A., 'Front-tracking method for viscous, incompressible, multi-fluid Flows', *J. Comp. Phys.* 100, 25-37, 1992.